

Microscopic theory of nonlinear Hall effect induced by electric field and temperature gradient

Terufumi Yamaguchi¹, Kazuki Nakazawa² and Ai Yamakage³

¹RIKEN Center for Emergent Matter Science, 2-1 Hirosawa, Wako, Saitama 351-0198, Japan

²Department of Applied Physics, University of Tokyo, Tokyo 113-8656, Japan

³Department of Physics, Nagoya University, Nagoya 464-8602, Japan



(Received 28 April 2023; accepted 18 April 2024; published 7 May 2024)

We investigate an intriguing phenomenon, the nonlinear chiral thermoelectric (NCTE) Hall effect, where electric current flows parallel to the outer product of an applied electric field and temperature gradient. We develop a general microscopic formulation and confirm the effect in a chiral crystal. Significantly, we find that the contribution of the orbital magnetic moment, which has been previously overlooked, is as crucial as the conventional Berry curvature dipole term. We further demonstrate a substantial NCTE Hall effect in a chiral Weyl semimetal. Our results shed new light on nonlinear transport phenomena and have broad implications for condensed matter physics.

DOI: [10.1103/PhysRevB.109.205117](https://doi.org/10.1103/PhysRevB.109.205117)

I. INTRODUCTION

Understanding quantum transport phenomena is essential in physics, as it allows us to determine the physical properties by observing how physical quantities respond to different external forces. We can also design and control materials and their structures based on the information on the transport coefficients for high-performance device applications. A typical example is the response of an electric current to an electric field: Ohm's law and the Hall effect [1] are historically well known, and the anomalous Hall effect [2–4] and the topological Hall effect [5–8] have been extensively studied in recent years. Employing a temperature gradient instead of an electric field, these phenomena are known as the Nernst effect and the anomalous (topological) Nernst effect [9–14]. These transport phenomena have been mainly studied as linear responses to external forces. On the other hand, there are responses to two or more external fields, namely nonlinear responses. Recently, nonlinear responses have been extensively studied, such as nonlinear optical responses, nonreciprocal transport, and the nonlinear Hall (Nernst) effect [15–29].

Here, we focus on the response of an electric current to the outer product of an electric field and a temperature gradient, which we call the nonlinear chiral thermoelectric (NCTE) Hall effect. The NCTE Hall effect is different from the superposition of linear responses: the direction of the NCTE Hall current changes when the direction of either an electric field or temperature gradient changes, whereas the direction does not change when the direction of both external forces changes (see Fig. 1). In other words, reversing the sign of one of the two “inputs” reverses the sign of the “output,” and reversing the sign of both “inputs” does not change the sign of the “output”; that is, it works the same as an XOR logic circuit.

The existence of the NCTE Hall effect has been predicted in Weyl fermion systems [30], and the description of the Berry curvature dipole has been obtained within semiclassical kinetic theory [31,32]. These studies have covered only Weyl systems and diverge at the low-temperature limit or have

only pointed out the possibility of the NCTE Hall effect. The microscopic formulation of the NCTE Hall effect for general band structures, verifying the finite NCTE Hall conductivities in concrete models and showing the NCTE Hall effect in actual crystals, is still absent.

This paper clarifies that the NCTE Hall effect occurs in chiral crystals, based on the microscopic theory we developed. First, we formulate the NCTE Hall effect microscopically by employing nonequilibrium (Keldysh) Green's functions [33] for the (nonlinear) responses not only to mechanical forces but also to the statistical forces. Next, by rewriting our formula in band representation within the relaxation time approximation, we find the novel terms expressed in the orbital magnetic moment adding to the conventional Berry curvature dipole terms. Applying our formula to a minimal model, we unveil the

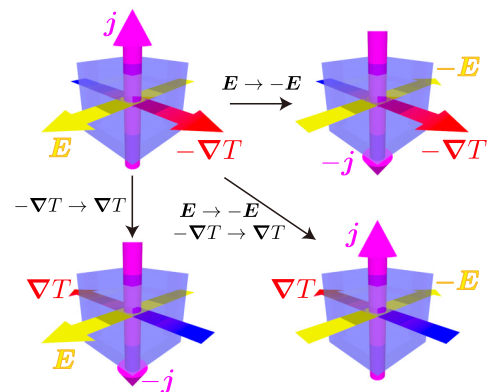


FIG. 1. Conceptual figure of the NCTE Hall effect. When applying an electric field \mathbf{E} and a temperature gradient $-\nabla T$ orthogonal to each other, a current \mathbf{j} flows perpendicular to both of them, $\mathbf{j} \propto \mathbf{E} \times (-\nabla T)$. Since the NCTE Hall effect is the nonlinear response, the sign of the current changes when replacing $\mathbf{E} \rightarrow -\mathbf{E}$ or $-\nabla T \rightarrow \nabla T$, whereas the sign is the same when replacing both $\mathbf{E} \rightarrow -\mathbf{E}$ and $-\nabla T \rightarrow \nabla T$.

finite NCTE Hall conductivity, in which the orbital magnetic moment terms are essential. Finally, we demonstrate the finite NCTE Hall conductivity in a model of chiral crystal proposed in Refs. [34,35], and obtain the NCTE Hall conductivity with experimentally measurable value.

II. FORMULATION OF THE NONLINEAR CHIRAL THERMOELECTRIC HALL EFFECT

We consider the Hamiltonian described as

$$\mathcal{H} = \mathcal{H}_0 + \mathcal{H}_{\text{imp}} + \mathcal{H}_{\text{ext}}, \quad (1)$$

$$\mathcal{H}_0 = \sum_k c_k^\dagger H_k c_k, \quad (2)$$

$$\mathcal{H}_{\text{imp}} = \int d\mathbf{r} c^\dagger(\mathbf{r}) V_{\text{imp}}(\mathbf{r}) c(\mathbf{r}), \quad (3)$$

$$\mathcal{H}_{\text{ext}} = e \int d\mathbf{r} \hat{n}(\mathbf{r}) \phi(\mathbf{r}, t), \quad (4)$$

where c^\dagger (c) is the creation (annihilation) operator, $V_{\text{imp}}(\mathbf{r})$ is the impurity potential, $e < 0$ is an electron charge, $\hat{n}(\mathbf{r}) = c^\dagger(\mathbf{r})c(\mathbf{r})$ is the number density operator, and $\phi(\mathbf{r}, t)$ is the scalar potential. Note that H_k is, in general, the spin and orbital space matrix. We define the retarded Green's function as

$$G_k^R(\varepsilon) = [\varepsilon - H_k - \Sigma_k^R(\varepsilon)]^{-1}, \quad (5)$$

where $\Sigma_k^R(\varepsilon)$ is the retarded self-energy due to the impurity scattering. We take the impurity average to retain the translational symmetry. The expectation value of physical quantity \hat{O} can be calculated by using the Keldysh Green's function as

$$\langle \hat{O} \rangle = -\frac{i}{2} \int \frac{d\varepsilon}{2\pi} \sum_k \text{tr}[\hat{O} G^K]. \quad (6)$$

To obtain the Keldysh Green's function, we calculate the Keldysh component of the Dyson equation,

$$G^K = G^R \star \Sigma^K \star G^A, \quad (7)$$

where the product \star is the star product which is equivalent to the convolution integral in the real time-space representation, or Moyal product in the Wigner representation. The self-energy of the Keldysh component is described with the local equilibrium distribution function as

$$\Sigma^K = \{1 - 2f_{\text{leq}}[\varepsilon; \mu, T(\mathbf{r})]\}(\Sigma^R - \Sigma^A), \quad (8)$$

$$f_{\text{leq}}[\varepsilon; \mu, T(\mathbf{r})] = \frac{1}{\exp[(\varepsilon - \mu)/T(\mathbf{r})] + 1}. \quad (9)$$

The response to the temperature gradient is obtained by taking the terms $\nabla T(\mathbf{r})$ from the Dyson equation (7). In linear response theory, the response to the temperature gradient is often calculated by introducing the gravitational potential [36]. The essence of this method is that one calculates the response to a gradient of gravitational potential based on the Kubo formula, and then replaces the gradient of gravitational potential with the temperature gradient for the nonequilibrium component using the Einstein-Luttinger relation. However, we note that the Einstein-Luttinger relation is only applicable near equilibrium states, namely, in the linear response regime. In other words, such a replacement is not justified in nonlinear

response regimes. In fact, violations of the Einstein-Luttinger relation in specific cases have been reported [37]. On the other hand, nonlinear responses to the temperature gradient are calculated based on the Boltzmann equations using the local equilibrium distribution function as the initial condition [16,38]. The method employed in this paper is analogous to the Boltzmann theory but is approached in a quantum mechanical framework, which allows for the incorporation of interband and topological contributions. We also incorporate an electric field by treating it in Keldysh space to obtain the nonlinear response to a temperature gradient and an electric field. For the latter convenience, we consider the setup in which the electric field and temperature gradient are applied to the xy plane. Generally, nonlinear conductivities are expressed in tensor form; however, it should be noted that for the NCTE Hall current, specifying the direction of the cross product between the electric field and the temperature gradient is sufficient. The NCTE Hall current j_z is expressed as

$$j_z = \sigma_z^{\text{NCTE}} \left[\mathbf{E} \times \left(-\frac{\nabla T}{T} \right) \right]_z, \quad (10)$$

with the NCTE Hall conductivity σ_z^{NCTE} ,

$$\begin{aligned} \sigma_z^{\text{NCTE}} = & -\frac{e^2}{4\pi} \int d\varepsilon \left(-\frac{\partial f}{\partial \varepsilon} \right) (\varepsilon - \mu) \sum_k \\ & \times \text{Im} \{ \text{tr} [v_z G^R v_x (\partial_\varepsilon G^R) v_y G^R \\ & + v_z (\partial_\varepsilon G^R) v_x G^R v_y G^A - v_z G^R v_x (\partial_\varepsilon G^R) v_y G^A \\ & - v_z G^R v_x G^R v_y (\partial_\varepsilon G^A)] - (v_x \leftrightarrow v_y) \}, \quad (11) \end{aligned}$$

where $v_i = \partial_{k_i} H_k$ is the velocity operator, and we put $G^{\text{R(A)}} = G_k^{\text{R(A)}}(\varepsilon)$ for simplicity. Here we assume that the spatial variation of the temperature $T(\mathbf{r})$ is slow and use the relation $(\partial_i f_{\text{leq}}) = (\partial_i T/T)(-\partial f/\partial \varepsilon)(\varepsilon - \mu)$ with (global) equilibrium distribution function $f(\varepsilon)$. The detailed derivation of the NCTE Hall current is shown in the Supplemental Material [39].

Equation (11) is one of the main results of this paper. By examining Eq. (11), we find that the NCTE Hall current becomes zero when the temperature reaches absolute zero, i.e., $T \rightarrow 0$. We can also find that the replacement part of the velocity operators “ $-(v_x \leftrightarrow v_y)$ ” in Eq. (11) is a critical factor for the NCTE Hall effect, which reflects that the NCTE Hall effect occurs only in the chiral materials. We can show from Eq. (10) that chiral is the only required symmetry for the NCTE Hall effect. Here the term “chiral” means the lack of symmetry with respect to any direction of mirror operation and spatial inversion. It is worth noting that, unlike the conventional (anomalous) Hall effect, the NCTE Hall effect does not necessarily require time-reversal breaking as an essential condition.

III. NCTE HALL EFFECT IN THE BAND REPRESENTATION

To describe the NCTE Hall current in the band representation, we introduce the unitary matrix $U_n(\mathbf{k})$, which diagonalizes H_k such that $U_n^\dagger(\mathbf{k}) H_k U_n(\mathbf{k}) = \varepsilon_{nk}$, where ε_{nk}

represents the eigenenergy of band n . We define the retarded Green's function in band representation as $G_{nk}^R(\varepsilon) = [\varepsilon - \varepsilon_{nk} + i\gamma]^{-1}$, where we assume the self-energy is written as $\Sigma^R = -i\gamma$. We drop any dependence on energy, momentum, and band indices for the damping rate γ . This assumption is essentially the same as in previous studies [31,32] by defining the relaxation time as $\tau = 1/(2\gamma)$. We obtain the NCTE Hall conductivity with $\sigma_z^{\text{NCTE}} = \sigma_z^{\text{BC}} + \sigma_z^{\text{OM}}$:

$$\sigma_z^{\text{BC}} = e^2 \tau \sum_{n,k} (\varepsilon_{nk} - \mu) \left(-\frac{\partial f}{\partial \varepsilon} \right)_{\varepsilon=\varepsilon_{nk}} \times \left[(\partial_z \varepsilon_{nk}) \Omega_n^z - \frac{1}{2} \{ (\partial_x \varepsilon_{nk}) \Omega_n^x + (\partial_y \varepsilon_{nk}) \Omega_n^y \} \right], \quad (12)$$

$$\sigma_z^{\text{OM}} = -\frac{e\tau}{2} \sum_{n,k} (\varepsilon_{nk} - \mu) \left(-\frac{\partial f}{\partial \varepsilon} \right)_{\varepsilon=\varepsilon_{nk}} \nabla_k \cdot \mathbf{m}_{nk}^\perp, \quad (13)$$

where $\Omega_n = \nabla \times \mathbf{A}_n(\mathbf{k})$ is the Berry curvature with the Berry connection $\mathbf{A}_n(\mathbf{k}) = -iU_n^\dagger(\mathbf{k})\nabla U_n(\mathbf{k})$, and $\mathbf{m}_{nk}^\perp = \mathbf{m}_{nk} - m_{nk}^z \hat{\mathbf{e}}_z = (m_{nk}^x, m_{nk}^y, 0)$ is the orbital magnetic moment which is written by the ‘‘interband Berry curvature’’ as

$$\mathbf{m}_{nk} = \frac{e}{2} \sum_m (\varepsilon_{mk} - \varepsilon_{nk}) \text{Im}[\mathbf{A}_{nm}(\mathbf{k}) \times \mathbf{A}_{mn}(\mathbf{k})], \quad (14)$$

where $\mathbf{A}_{nm}(\mathbf{k}) = -iU_n^\dagger \nabla U_m$ is the ‘‘interband Berry connection.’’ Equation (14) is equivalent to the expression used in Ref. [35]. σ_z^{BC} can be expressed by the Berry curvature dipole which has been discussed within semiclassical theory [31,32]. On the other hand, σ_z^{OM} is a novel term that we have identified, which is comparable with the conventional term σ_z^{BC} in terms of the relaxation time τ . Both σ_z^{BC} and σ_z^{OM} are expressed as products of the same direction of wave vector derivatives and Berry curvature or orbital magnetic moment, which are different from the conventional nonlinear Hall effect [15,17,18,24–26]. In fact, σ_z^{OM} can be understood as a Nernst effect arising from the nonequilibrium orbital magnetization induced in the direction of the applied electric field [40–42]; see the Supplemental Material [39]. In the following, we show that σ_z^{OM} is essential in a concrete model. We note that there is no need to assume the (constant) relaxation time approximation in Eq. (11), since all contributions, such as energy and wave number dependencies, can be taken into account naturally by calculating the self-energy and corresponding vertex corrections. We also note that we can incorporate lower-order relaxation time (higher-order damping constant), including τ^0 contributions, in Eq. (11); see details in the Supplemental Material [39]. This feature distinguishes our microscopic formulation from semiclassical analyses, in which only τ^1 contributions appear in the DC limit.

IV. ANALYSIS IN THE MINIMAL MODEL

Here we give a minimal model in which the finite NCTE Hall conductivity arises. This model consists of the Weyl electrons (linear in wave vector) with a term of second order in wave vector, which is written as

$$H_{\mathbf{k}} = v_F \mathbf{k} \cdot \boldsymbol{\sigma} + \lambda k^2, \quad (15)$$

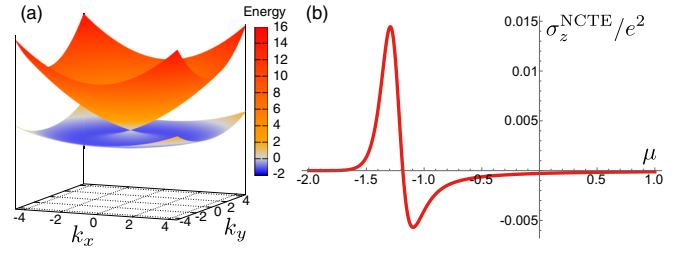


FIG. 2. (a) Band structure of Hamiltonian (15) at $k_z = 0$. (b) The chemical potential dependence of the NCTE Hall conductivity at temperature $T = 0.05$. Here we fix the parameters as $v_F = 1$, $\lambda = 0.2$, and $\gamma = 0.1$.

where v_F is the Fermi velocity, $\boldsymbol{\sigma} = (\sigma^x, \sigma^y, \sigma^z)$ are the Pauli matrices, and λ represents the strength of a term proportional to k^2 . This model holds the time-reversal symmetry, and the anomalous Hall effect does not occur. The eigenenergy ε_{\pm} and eigenvectors \mathbf{u}_{\pm} are given as $H_{\mathbf{k}} \mathbf{u}_{\pm} = \varepsilon_{\pm} \mathbf{u}_{\pm}$ with

$$\varepsilon_{\pm} = \lambda k^2 \pm v_F k, \quad (16)$$

$$\mathbf{u}_+ = \begin{pmatrix} \cos \frac{\theta}{2} e^{-i\varphi/2} \\ \sin \frac{\theta}{2} e^{i\varphi/2} \end{pmatrix}, \quad (17)$$

$$\mathbf{u}_- = \begin{pmatrix} \sin \frac{\theta}{2} e^{-i\varphi/2} \\ -\cos \frac{\theta}{2} e^{i\varphi/2} \end{pmatrix}, \quad (18)$$

where we introduce the polar coordinates (k, θ, φ) with $k_x = k \sin \theta \cos \varphi$, $k_y = k \sin \theta \sin \varphi$, $k_z = k \cos \theta$. The energy band structure at $k_z = 0$ is shown in Fig. 2(a). The eigenvectors in this model are the same as in the Weyl model, and we can calculate the Berry curvature and the orbital magnetic moment,

$$\Omega_{\pm} = \pm \frac{\mathbf{k}}{k^3}, \quad (19)$$

$$\mathbf{m}_{\pm} = -\frac{e v_F \mathbf{k}}{2 k^2}. \quad (20)$$

Substituting (19), (20), and the velocity $v_{\pm,j} = \partial_{k_j} \varepsilon_{\pm} = (2\lambda \pm v_F/k) k_j$ in (12) and (13), we obtain the NCTE Hall conductivities

$$\sigma_z^{\text{BC}} = 0, \quad (21)$$

$$\sigma_z^{\text{OM}} = \frac{e^2 v_F \tau}{6\pi^2} \int_{-\frac{v_F}{4\lambda}}^{\infty} d\varepsilon \frac{\varepsilon - \mu}{\sqrt{v_F^2 + 4\lambda\varepsilon}} \left(-\frac{\partial f}{\partial \varepsilon} \right). \quad (22)$$

We find that the contribution from the Berry curvature dipole disappears, while the contribution from the orbital magnetic moment is essential. The dependence of the NCTE Hall conductivity on the chemical potential is shown in Fig. 2(b). Although the orbital magnetic moment arises near the ‘‘Weyl point’’ $\varepsilon_k = 0$, the NCTE Hall conductivity is enhanced when we tune the chemical potential near the bottom of the lower energy band. This enhancement reflects the nature of thermoelectric transport, $\int d\varepsilon (-\partial_{\varepsilon} f)(\varepsilon - \mu) \dots$, which is enhanced when the chemical potential is near a sharp singularity in the density of states [43]. We can see that the NCTE Hall effect is zero in the linear model, including the linear Weyl model

where the Berry curvature and the orbital magnetic moment are as described by Eqs. (21) and (22); see the Supplemental Material [39]. We can also see that $\sigma_z^{\text{OM}} = 0$ when $\lambda \rightarrow 0$, at which point the Hamiltonian reduces to the linear Weyl model $H_{\mathbf{k}} = v_F \mathbf{k} \cdot \boldsymbol{\sigma}$. We emphasize that we need to consider not only the enhancement of the Berry curvature dipoles or the orbital magnetic moment but also the differentials of the density of states to obtain the large NCTE Hall conductivity. One might think that the NCTE Hall conductivity in Eq. (22) will become zero in a crystal since it is proportional to v_F and is canceled by considering the pair of Weyl points. We should note that these Weyl points are generally located at different energies; here we put the energy difference as μ_5 . Since the NCTE Hall conductivity is proportional to the derivative of Fermi distribution function, the single Weyl model is valid when $\mu_5 \gg k_B T$. Moreover, even when considering both Weyl points, $\sigma_z^{\text{NCTE}}|_{\mu+\mu_5} - \sigma_z^{\text{NCTE}}|_{\mu}$ generally holds a finite value. In fact, we show the finite NCTE Hall conductivity in a chiral crystal model hereafter.

V. NCTE HALL EFFECT IN CHIRAL CRYSTAL MODEL

Here we demonstrate that the NCTE Hall effect can be realized in crystals. As mentioned above, the only required symmetry for the NCTE Hall effect is chiral, which implies that the NCTE Hall effect can be realized in trigonal Te and Se [44]. In this paper, we employ the model of a chiral Weyl semimetal [45]. We consider the tight-binding model proposed in Refs. [34,35], which consists of an infinite stack of honeycomb lattice layers, and describe the Bloch Hamiltonian as

$$H_{\mathbf{k}} = d_0 + \mathbf{d}_{\mathbf{k}} \cdot \boldsymbol{\sigma}, \quad (23)$$

$$d_0 = 2t_2 \cos(k_z c) \sum_i \cos(\mathbf{k} \cdot \mathbf{b}_i) + 2t_3 \cos(k_z c), \quad (24)$$

$$d_x = t_1 \sum_i \cos(\mathbf{k} \cdot \mathbf{a}_i), \quad (25)$$

$$d_y = t_1 \sum_i \sin(\mathbf{k} \cdot \mathbf{a}_i), \quad (26)$$

$$d_z = -2t_2 \sin(k_z c) \sum_i \sin(\mathbf{k} \cdot \mathbf{b}_i), \quad (27)$$

where $\mathbf{d}_{\mathbf{k}} = (d_x, d_y, d_z)$, $\boldsymbol{\sigma} = (\sigma^x, \sigma^y, \sigma^z)$ are the Pauli matrices, $\mathbf{a}_1 = a/\sqrt{3}\hat{e}_y$, $\mathbf{a}_2 = a/2\hat{e}_x - a/(2\sqrt{3})\hat{e}_y$, $\mathbf{a}_3 = -a/2\hat{e}_x - a/(2\sqrt{3})\hat{e}_y$, $\mathbf{b}_1 = a\hat{e}_x$, $\mathbf{b}_2 = -a/2\hat{e}_x + a\sqrt{3}/2\hat{e}_y$, $\mathbf{b}_3 = -a/2\hat{e}_x - a\sqrt{3}/2\hat{e}_y$, t_1, t_2, t_3 are the hopping parameters, and a and c are the intralayer and interlayer lattice constants, respectively. We plot the energy bands and the density of states of the Hamiltonian (23) in Figs. 3(a) and 3(b), respectively. (The parameters we use in the calculation are shown in the caption of Fig. 3.) There are Weyl points at the K and H points, and the Berry curvature and the orbital magnetic moment are enhanced around the Weyl nodes, as shown in Fig. 4. To obtain the NCTE Hall conductivity, we apply the Sommerfeld expansion and evaluate the lowest order in temperature T , assuming a low-temperature limit. We also assume a constant and pure

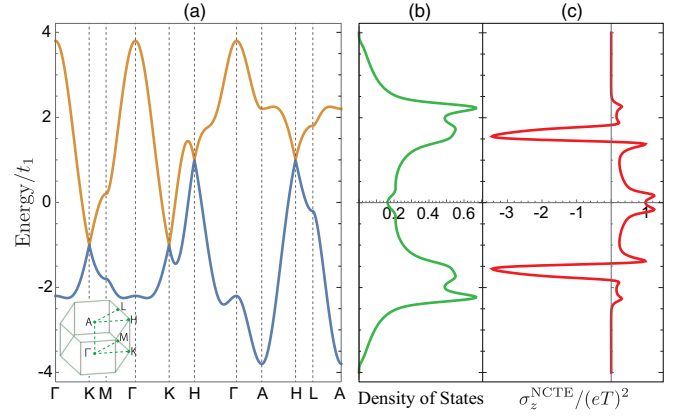


FIG. 3. (a) Energy bands and (b) density of states of the Hamiltonian (23). (c) The NCTE Hall conductivity within the lowest order in Sommerfeld expansion as a function of the chemical potential. We use the parameters $a = 1.0$, $c = 1.0$, $t_1 = 1.0$, $t_2 = 0.2$, $t_3 = -0.2$, and $\gamma = 0.1$.

imaginary self-energy $\Sigma^{\text{R}} = -i\gamma$. In Fig. 3(c), we plot the NCTE Hall conductivity of this model at a low temperature as a function of the chemical potential. We find a finite NCTE Hall conductivity in a wide range of the chemical potential, with an enhancement of the NCTE Hall conductivity near the Weyl points and at points where the density of states varies sharply, which is consistent with the discussion in the minimal model. We estimate the NCTE Hall conductivity in this model using realistic parameters. In Fig. 3(c), we set $\gamma/t_1 = 0.1$ for numerical calculation, which is too large for a realistic situation. As given in Eq. (11), we assume that the NCTE Hall conductivity is proportional to $\tau = \hbar/(2\gamma)$ and set $\gamma/t_1 = 0.001$ for estimation. Assuming a temperature gradient $\nabla T/T \simeq 10^2 \text{ m}^{-1}$, an electric field $E \simeq 10^3 \text{ V/m}$, and a system size $L \times L \times L$ with $L \simeq 1.0 \text{ }\mu\text{m}$, we obtain an NCTE Hall conductivity of order $\sigma_z^{\text{NCTE}} \sim 10e^2/h$ and corresponding NCTE Hall current of order $j_z \sim 100 \text{ pA}$, which are experimentally measurable.

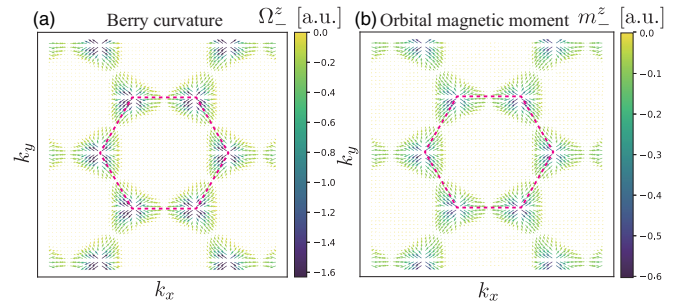


FIG. 4. (a) The Berry curvature and (b) the orbital magnetic moment of the lower band at $k_z = \pi - \delta$, where we put the small quantity $\delta = 3\pi/160$ to avoid the singular points. The lengths of arrows represent their magnitude in the k_x - k_y plane, and color represents their magnitude in the k_z direction. Dashed lines represent the boundary of the Brillouin zones. Both the Berry curvature and the orbital magnetic moment are enhanced near the H points.

VI. CONCLUSION

In this paper, we have formulated the NCTE Hall effect using the method of quantum field theory at the microscopic level. By rewriting the formula in the band representation, we have identified the contributions of the orbital magnetic moment in addition to the Berry curvature dipole contributions. Through analysis of the minimal model, we have demonstrated the essential nature of the contribution of the orbital magnetic moment to the NCTE Hall effect. Our findings show that the chiral crystal model gives rise to finite NCTE Hall conductivity. These results provide important insights into the

understanding of nonlinear transport phenomena and pave the way for further investigations in this field.

ACKNOWLEDGMENTS

We acknowledge G. Qu and E. Saitoh for valuable discussion. A.Y. is supported by JSPS KAKENHI (Grant No. JP20K03835) and the Sumitomo Foundation (Grant No. 190228). K.N. is supported by JSPS KAKENHI (Grant No. JP21K13875). T.Y. is supported by JSPS KAKENHI (Grant No. JP21K14526).

-
- [1] E. H. Hall, On a new action of the magnet on electric currents, *Am. J. Math.* **2**, 287 (1879).
- [2] N. A. Sinitsyn, Semiclassical theories of the anomalous Hall effect, *J. Phys.: Condens. Matter* **20**, 023201 (2008).
- [3] N. Nagaosa, J. Sinova, S. Onoda, A. H. MacDonald, and N. P. Ong, Anomalous Hall effect, *Rev. Mod. Phys.* **82**, 1539 (2010).
- [4] C.-Z. Chang, J. Zhang, X. Feng, J. Shen, Z. Zhang, M. Guo, K. Li, Y. Ou, P. Wei, L.-L. Wang, Z.-Q. Ji, Y. Feng, S. Ji, X. Chen, J. Jia, X. Dai, Z. Fang, S.-C. Zhang, K. He, Y. Wang *et al.*, Experimental observation of the quantum anomalous Hall effect in a magnetic topological insulator, *Science* **340**, 167 (2013).
- [5] P. Bruno, V. K. Dugaev, and M. Taillefumier, Topological Hall effect and Berry phase in magnetic nanostructures, *Phys. Rev. Lett.* **93**, 096806 (2004).
- [6] G. Tatara and H. Kawamura, Chirality-driven anomalous Hall effect in weak coupling regime, *J. Phys. Soc. Jpn.* **71**, 2613 (2002).
- [7] A. Neubauer, C. Pfleiderer, B. Binz, A. Rosch, R. Ritz, P. G. Niklowitz, and P. Böni, Topological Hall effect in the A phase of MnSi, *Phys. Rev. Lett.* **102**, 186602 (2009).
- [8] K. Nakazawa, M. Bibes, and H. Kohno, Topological Hall effect from strong to weak coupling, *J. Phys. Soc. Jpn.* **87**, 033705 (2018).
- [9] R. Suryanarayanan, V. Gasumyants, and N. Ageev, Anomalous Nernst effect in $\text{La}_{0.88}\text{MnO}_3$, *Phys. Rev. B* **59**, R9019 (1999).
- [10] W.-L. Lee, S. Watauchi, V. L. Miller, R. J. Cava, and N. P. Ong, Anomalous Hall heat current and Nernst effect in the $\text{CuCr}_2\text{Se}_{4-x}\text{Br}_x$ ferromagnet, *Phys. Rev. Lett.* **93**, 226601 (2004).
- [11] N. Hanasaki, K. Sano, Y. Onose, T. Ohtsuka, S. Iguchi, I. Kézsmárki, S. Miyasaka, S. Onoda, N. Nagaosa, and Y. Tokura, Anomalous Nernst effects in pyrochlore molybdates with spin chirality, *Phys. Rev. Lett.* **100**, 106601 (2008).
- [12] M. Mizuguchi and S. Nakatsuji, Energy-harvesting materials based on the anomalous Nernst effect, *Sci. Technol. Adv. Mater.* **20**, 262 (2019).
- [13] Y. Shiomi, N. Kanazawa, K. Shibata, Y. Onose, and Y. Tokura, Topological Nernst effect in a three-dimensional skyrmion-lattice phase, *Phys. Rev. B* **88**, 064409 (2013).
- [14] Y. P. Mizuta and F. Ishii, Large anomalous Nernst effect in a skyrmion crystal, *Sci. Rep.* **6**, 28076 (2016).
- [15] I. Sodemann and L. Fu, Quantum nonlinear Hall effect induced by Berry curvature dipole in time-reversal invariant materials, *Phys. Rev. Lett.* **115**, 216806 (2015).
- [16] R. Takashima, Y. Shiomi, and Y. Motome, Nonreciprocal spin Seebeck effect in antiferromagnets, *Phys. Rev. B* **98**, 020401(R) (2018).
- [17] S. Nandy and I. Sodemann, Symmetry and quantum kinetics of the nonlinear Hall effect, *Phys. Rev. B* **100**, 195117 (2019).
- [18] D. E. Parker, T. Morimoto, J. Orenstein, and J. E. Moore, Diagrammatic approach to nonlinear optical response with application to Weyl semimetals, *Phys. Rev. B* **99**, 045121 (2019).
- [19] Q. Ma, S.-Y. Xu, H. Shen, D. MacNeill, V. Fatemi, T.-R. Chang, A. M. Mier Valdivia, S. Wu, Z. Du, C.-H. Hsu, S. Fang, Q. D. Gibson, K. Watanabe, T. Taniguchi, R. J. Cava, E. Kaxiras, H.-Z. Lu, H. Lin, L. Fu, N. Gedik *et al.*, Observation of the nonlinear Hall effect under time-reversal-symmetric conditions, *Nature (London)* **565**, 337 (2019).
- [20] X.-Q. Yu, Z.-G. Zhu, J.-S. You, T. Low, and G. Su, Topological nonlinear anomalous Nernst effect in strained transition metal dichalcogenides, *Phys. Rev. B* **99**, 201410(R) (2019).
- [21] C. Zeng, S. Nandy, A. Taraphder, and S. Tewari, Nonlinear Nernst effect in bilayer WTe_2 , *Phys. Rev. B* **100**, 245102 (2019).
- [22] H. Ishizuka and N. Nagaosa, Anomalous electrical magnetochiral effect by chiral spin-cluster scattering, *Nat. Commun.* **11**, 2986 (2020).
- [23] C. Zeng, S. Nandy, and S. Tewari, Fundamental relations for anomalous thermoelectric transport coefficients in the nonlinear regime, *Phys. Rev. Res.* **2**, 032066(R) (2020).
- [24] Y. Michishita and R. Peters, Effects of renormalization and non-Hermiticity on nonlinear responses in strongly correlated electron systems, *Phys. Rev. B* **103**, 195133 (2021).
- [25] Z. Z. Du, H.-Z. Lu, and X. C. Xie, Nonlinear Hall effects, *Nat. Rev. Phys.* **3**, 744 (2021).
- [26] Z. Z. Du, C. M. Wang, H.-P. Sun, H.-Z. Lu, and X. C. Xie, Quantum theory of the nonlinear Hall effect, *Nat. Commun.* **12**, 5038 (2021).
- [27] C. Zeng, S. Nandy, and S. Tewari, Chiral anomaly induced nonlinear Nernst and thermal Hall effects in Weyl semimetals, *Phys. Rev. B* **105**, 125131 (2022).
- [28] C. Zeng, X.-Q. Yu, Z.-M. Yu, and Y. Yao, Band tilt induced nonlinear Nernst effect in topological insulators: An efficient generation of high-performance spin polarization, *Phys. Rev. B* **106**, L081121 (2022).
- [29] Y. D. Wang, Z.-G. Zhu, and G. Su, Quantum theory of nonlinear thermal response, *Phys. Rev. B* **106**, 035148 (2022).

- [30] Y. Hidaka, S. Pu, and D.-L. Yang, Nonlinear responses of chiral fluids from kinetic theory, *Phys. Rev. D* **97**, 016004 (2018).
- [31] R. Nakai and N. Nagaosa, Nonreciprocal thermal and thermoelectric transport of electrons in noncentrosymmetric crystals, *Phys. Rev. B* **99**, 115201 (2019).
- [32] R. Toshio, K. Takasan, and N. Kawakami, Anomalous hydrodynamic transport in interacting noncentrosymmetric metals, *Phys. Rev. Res.* **2**, 032021(R) (2020).
- [33] A. Kamenev, *Field Theory of Non-Equilibrium Systems* (Cambridge University Press, Cambridge, 2011).
- [34] T. Yoda, T. Yokoyama, and S. Murakami, Current-induced orbital and spin magnetizations in crystals with helical structure, *Sci. Rep.* **5**, 12024 (2015).
- [35] T. Yoda, T. Yokoyama, and S. Murakami, Orbital Edelstein effect as a condensed-matter analog of solenoids, *Nano Lett.* **18**, 916 (2018).
- [36] J. M. Luttinger, Theory of thermal transport coefficients, *Phys. Rev.* **135**, A1505 (1964).
- [37] J. Park, O. Golan, Y. Vinkler-Aviv, and A. Rosch, Thermal Hall response: Violation of gravitational analogs and Einstein relations, *Phys. Rev. B* **105**, 205419 (2022).
- [38] K. Nakazawa, Y. Kato, and Y. Motome, Asymmetric modulation of Majorana excitation spectra and nonreciprocal thermal transport in the Kitaev spin liquid under a staggered magnetic field, *Phys. Rev. B* **105**, 165152 (2022).
- [39] See Supplemental Material at <http://link.aps.org/supplemental/10.1103/PhysRevB.109.205117> for the details of the method of treating the temperature gradient in nonlinear responses, derivation of the nonlinear chiral thermoelectric Hall current, details of the NCTE Hall effect, and proof of the zero NCTE Hall conductivity in the linear (anisotropic Weyl electron) model.
- [40] S. Zhong, J. E. Moore, and I. Souza, Gyrotropic magnetic effect and the magnetic moment on the Fermi surface, *Phys. Rev. Lett.* **116**, 077201 (2016).
- [41] C. Xiao, H. Liu, J. Zhao, S. A. Yang, and Q. Niu, Thermoelectric generation of orbital magnetization in metals, *Phys. Rev. B* **103**, 045401 (2021).
- [42] A. Widom, Thermodynamic derivation of the Hall effect current, *Phys. Lett. A* **90**, 474 (1982).
- [43] G. D. Mahan and J. O. Sofo, The best thermoelectric, *Proc. Natl. Acad. Sci. USA* **93**, 7436 (1996).
- [44] M. Hirayama, R. Okugawa, S. Ishibashi, S. Murakami, and T. Miyake, Weyl node and spin texture in trigonal tellurium and selenium, *Phys. Rev. Lett.* **114**, 206401 (2015).
- [45] N. P. Armitage, E. J. Mele, and A. Vishwanath, Weyl and Dirac semimetals in three-dimensional solids, *Rev. Mod. Phys.* **90**, 015001 (2018).